Doppler Centroid Estimation with Quality Assessment for Real-Time SAR Imaging

Yu-Chieh Lee[1], Pei-Yun Tsai[1], and Sz-Yuan Lee[2]
[1]Department of Electrical Engineering, National Central University, Taiwan
[2]National Space Program Office, National Applied Research Laboratory, Taiwan

***Abstract*—The range Doppler algorithm (RDA) is widely used for synthetic aperture radar (SAR) imaging. Correct estimation for Doppler centroid is essential for range cell migration correction, azimuth compression, secondary range compression in RDA. This paper presents two methods to assess and improve the Doppler parameter estimation results. The symmetry of the Doppler spectrum is examined to evaluate the quality of coarse estimation of baseband Doppler centroid and the weighted least squares algorithm is used to derive the refined results. Selective window and weighted combining based on the quality index of the average power are adopted for detecting Doppler ambiguity. From the simulation results, we show that the proposed techniques with the appropriate quality index can improve the performance of estimation compared to the conventional schemes for real-time SAR signal processing.**

***Index Terms*—Synthetic Aperture Radar, Doppler centroid estimation, Doppler ambiguity.**

I. INTRODUCTION

Rapid development of synthetic aperture radar technology is shown during these decades. It has been used in many fields. Operating in all weather, all day and night, SAR systems can support earth observation and military surveillance. Various algorithms have been proposed to process SAR signals for imaging, such as range Doppler algorithm (RDA) and Chirp Scaling algorithm (CSA) [1]. In RDA, once SAR signals are transformed by azimuth FFT, accurate Doppler centroid is required for secondary range compression (SRC), range cell migration correction (RCMC), and azimuth compression. In CSA, the azimuth FFT is first applied to the received SAR signals. All the remaining steps, including differential RCMC, bulk RCMC, etc., rely on the information defined in the Doppler spectrum. Consequently, inaccurate Doppler centroid estimation results in degradation of image quality.

Although Doppler centroid can be calculated from the attitude information of the SAR system, uncertainties exist during the measurement. Hence, many approaches have been proposed to estimate Doppler centroid from the received echo signals [2][3][4]. To acquire correct Doppler centroid, baseband Doppler centroid and Doppler ambiguity are required [1]. The average cross correlation coefficient (ACCC) method computes the average of phase increment [2] between the adjacent azimuth samples to derive the baseband Doppler centroid. However, if the reflected signal is weak or the contrast of the scenes is high, the acquired phase will likely be wrong and inaccurate estimate will be generated.

In the multi-look beat frequency (MLBF) algorithm [3], the whole range spectrum is partitioned into two range looks. The beat frequency, from the response of a scatter at two different transmitted frequencies, is proportional to the Doppler centroid and thus can be obtained by Fourier transform. The multi-look cross-correlation (MLCC) algorithm calculates ACCC of two looks and examines the phase difference to derive the Doppler centroid. It has been mentioned in [3] that the MLCC is suitable for low-contrast scenes. In [4], virtual multi-channel SAR data are generated and the antenna pattern is obtained by Capon spectral estimator. The Doppler centroid is estimated by Curve fitting. In [5], a Radon transform-based Doppler parameter estimator has been proposed. It employs an average over a number of range bins. Although the performance of Radon transform is good, its heavy computations may not be suitable for real-time processing [6].

In this paper, we propose two low-complexity schemes to assess and improve the estimation accuracy of baseband Doppler centroid and Doppler ambiguity for real-time SAR imaging. The quality of the estimation result is assessed and only reliable results are taken into consideration. Besides, the SNR is used as weighting and the weighted least squares algorithm is employed for baseband Doppler centroid estimation. As to the Doppler ambiguity, techniques of the selective window and weighted combination are applied. From the simulation results, the proposed techniques can improve the estimation accuracy compared to the conventional methods.

II. SYSTEM MODEL FOR DOPPLER CENTROID ESTIMATION

The flow of RDA with the procedure of Doppler parameter estimation by MLBF and ACCC is described in Fig. 1. The received SAR signal $s_{bb}(\tau,\eta)$ is first transformed into the range frequency domain and becomes $s_{bb}(f_\tau,\eta)$. After range compression, in order to support real-time processing, Doppler parameter estimation is activated as shown in the left part. For baseband Doppler centroid estimation, the range-compressed frequency domain signal $s_{rc}(f_\tau,\eta)$ is transformed back to the range time domain and $s_{rc}(\tau,\eta)$ is obtained. The ACCC is calculated by [1]

$$\Gamma = \sum_\tau \sum_\eta s_{rc}{}^*(\tau,\eta) s_{rc}(\tau,\eta+\Delta\eta) \quad (1)$$

where $\Delta\eta = 1/F_a$, the inverse of the pulse repetition frequency. The initial baseband Doppler centroid $\hat{f}'_{\eta_c}$ is then estimated by

$$\hat{f}'_{\eta_c} = \frac{F_a}{2\pi}\angle\Gamma. \quad (2)$$

As shown in Fig. 2, for detection of Doppler ambiguity, the data in the range frequency and azimuth time domain are partitioned into two looks, one in the positive frequency band and the other in the negative frequency band with a spacing of $\Delta f_\tau = B_\tau/2$, where B_τ is the signal bandwidth in the range frequency domain. Regardless of amplitude attenuation, the range compressed data in the azimuth domain of two looks take the form of

$$s_{l_1}(\eta) = \omega_a(\eta-\eta_c)\cdot exp\left\{-j\frac{4\pi}{c}\left(f_0 - \frac{\Delta f_\tau}{2}\right)R(\eta)\right\} \quad (3)$$

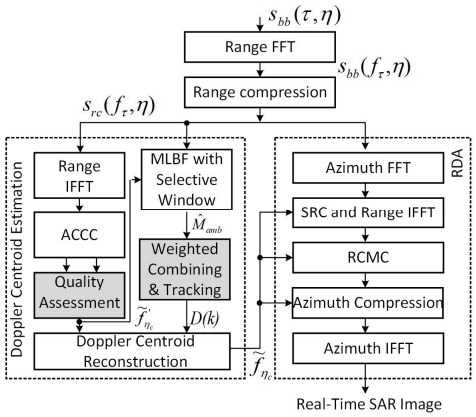

Fig. 1 SAR data processing flow with MLBF and RDA.

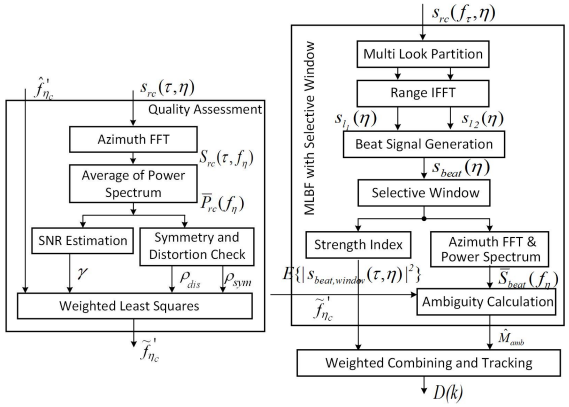

(a) (b)

Fig. 2 Processing flow of (a) quality assessment and (b) MLBF with selective window.

and

$$s_{l_2}(\eta) = \omega_a(\eta - \eta_c) \cdot exp\left\{-j\frac{4\pi}{c}\left(f_0 + \frac{\Delta f_\tau}{2}\right)R(\eta)\right\}. \quad (4)$$

where $R(\eta)$ represents the distance between the radar and the target at azimuth time η, $\omega_a(\cdot)$ represents two-way antenna pattern, f_0 is radar center frequency. The beat signal is calculated by

$$s_{beat}(\eta) = {s_{l_1}}^*(\eta)s_{l_2}(\eta). \quad (5)$$

Applying Fourier transform to $s_{beat}(\eta)$, we get its power spectrum $S_{beat}(f_\eta)$. Define

$$\bar{S}_{beat}(f_\eta) = |\mathbb{E}_\tau\{S_{beat}(f_\eta)\}|^2.$$
$$f_{beat} = arg\ max_{f_\eta}\ \bar{S}_{beat}(f_\eta). \quad (6)$$

The Doppler centroid $\hat{f}_{\eta_c}$ is first calculated by

$$\hat{f}_{\eta_c} = \frac{f_0}{\Delta f_\tau} f_{beat}, \quad (7)$$

and Doppler ambiguity $\hat{M}_{amb}$ is then detected by

$$\hat{M}_{amb} = round(\frac{\hat{f}_{\eta_c} - \tilde{f}'_{\eta_c}}{F_a}), \quad (8)$$

with the refined baseband Doppler centroid $\tilde{f}'_{\eta_c}$. The Doppler centroid $\tilde{f}_{\eta_c}$ is then reconstructed by

$$\tilde{f}_{\eta_c} = \hat{M}_{amb} \cdot F_a + \tilde{f}'_{\eta_c}. \quad (9)$$

III. Improvement of Doppler Centroid Estimation in Real-Time Processing

In [1], the authors have mentioned that due to the contrast of the scenes and the reflected signal strength, the estimation results must be assessed by some quality indexes, such as signal-to-noise ratio (SNR), contrast, and spectrum distortion. Furthermore, for real-time processing, the received SAR signals must be partitioned into blocks each using a moderate FFT size. Hence, it is infeasible to check the estimation results after processing a large-scale region. In order to obtain real-time SAR imaging with good performance, a fast and low-complexity estimation approach must be adopted for Doppler centroid estimation.

In Fig. 2, we show the detailed flow of our Doppler centroid estimation. Since ACCC for baseband Doppler centroid is sensitive to high-contrast scenes and low SNR, the quality of initial estimate $\hat{f}'_{\eta_c}$ is evaluated by checking the symmetry and distortion of the Doppler power spectrum. The weighted least squares (WLS) algorithm is adopted to derive the refined estimates according to the SNR value. Furthermore, the MLBF algorithm is suitable for high-contrast scenes. Thus, we propose a selective window technique to choose the region with the strongest reflection in each image block. Since the Doppler ambiguity does not vary too much among adjacent image blocks, the weighted combination is proposed for $\hat{M}_{amb}$ to improve the performance of the final Doppler centroid reconstruction. Details will be illustrated in the following.

A. Assessment of baseband Doppler centroid estimation

Usually in the scenes with uniform scattering, the Doppler power spectrum is symmetric and highly related with the beam pattern [1][7]. Hence, if there exist high-contrast scenes, skewed Doppler power spectrum will be obtained. In [1], curve fitting is suggested and the mean square error (MSE) of the averaged spectrum and the fitting curve is adopted to check the distortion. In [7], the coherence information and polynomial surface fitting are used. Here, we use moving average to smoothen the power spectrum. In addition to the spectrum distortion mentioned in [1], we propose to include the spectrum symmetry for quality assessment.

As shown in Fig. 2(a), given the signal $S_{rc}(\tau, f_\eta)$ in the range Doppler domain after range compression, the average power spectrum is computed by

$$\bar{P}_{rc}(f_\eta) = |\sum_\tau S_{rc}(\tau, f_\eta)|^2. \quad (10)$$

The moving average filter is defined as

$$H(f_\eta) = \begin{cases} 1 & f_\eta \in [-\frac{B_{mov}}{2}, \frac{B_{mov}}{2}] \\ 0 & otherwise \end{cases} \quad (11)$$

and $\bar{Q}_{rc}(f_\eta) = H(f_\eta) \otimes \bar{P}_{rc}(f_\eta)$, where $\otimes$ denotes the circular convolution and B_{mov} is the length of moving average.

In the conventional method [1], the distortion of $\bar{P}_{rc}(f_\eta)$ is examined by calculating root-mean-square error (RMSE) between $\bar{P}_{rc}(f_\eta)$ and the smoothened curve, $\bar{Q}_{rc}(f_\eta)$ [1],

$$\epsilon_{dis} = \sqrt{\sum_{f_\eta}[\bar{Q}_{rc}(f_\eta) - \bar{P}_{rc}(f_\eta)]^2}. \quad (12)$$

Due to reflectivity difference of the ocean and land, skewness of $\bar{P}_{rc}(f_\eta)$ exists. We suggest to evaluate the symmetry of $\bar{Q}_{rc}(f_\eta)$ by comparing the waveform difference relative to peak after moving average,

$$\epsilon_{sym} = \sqrt{\sum_{\Delta f_\eta} |\bar{Q}_{rc}([f_p + \Delta f_\eta]_{F_a}) - \bar{Q}_{rc}([f_p - \Delta f_\eta]_{F_a})|^2}, \quad (13)$$

where $f_p = \arg max_f \ \bar{Q}_{rc}(f_\eta)$, $\Delta f_\eta \in [0, F_a/2]$, and $[\cdot]_{F_a}$ denotes modulo-F_a operation. Given that the noise power is approximated by $P_n \approx \bar{Q}_{rc}(f_p + F_a/2)$ in the Doppler spectrum, the signal power P_s is derived from the average of $\bar{Q}_{rc}(f_\eta) - P_n$. The SNR is approximated by $\gamma = \frac{P_s}{P_n}$. The distortion index is defined by

$$\rho_{dis} = \frac{\epsilon_{dis}}{P_s} * 100\%, \quad (14)$$

and the symmetry index takes the form of

$$\rho_{sym} = \frac{\epsilon_{sym}}{P_s} * 100\%. \quad (15)$$

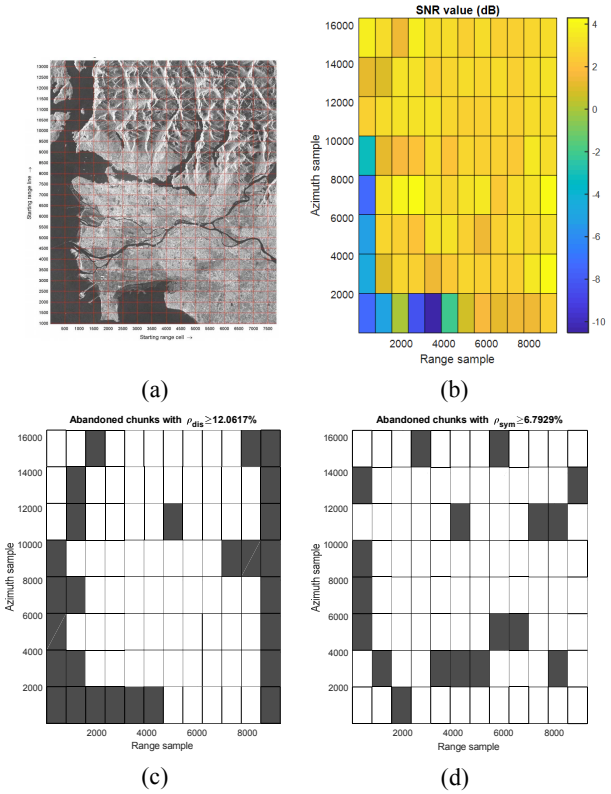

Fig. 4 (a) RADARSAT signals from Canada region [1], (b) the SNR value, (c) assessment by ρ_{dis}, and (d) assessment by ρ_{sym}.

Table I System parameters [1].

$F_a(Hz)$	1256.98	$K_r\ (Hz/s)$	7.2135×10^7
$F_r(Hz)$	3.2317×10^7	$T_r\ (sec)$	4.175×10^{-5}
$f_0\ (Hz)$	5.3×10^9	$V_r\ (m/s)$	7062
$R_0(m)$	998647	$L_a(m)$	15
B_{mov}(Hz)	200	N_a	2048
N_r	4644	N_{chunk}	774

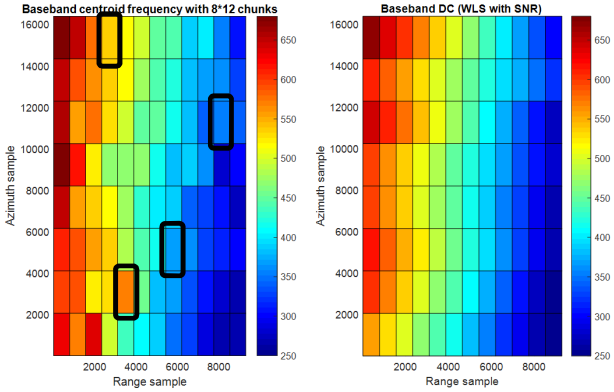

Fig. 5 (a) Estimation results without quality assessment, and (b) estimation results by weighted least squares after quality assessment.

We then use RADARSAT signal [1] to examine the feasibility of the proposed scheme. The system parameters are listed in Table I, where F_r is the sampling frequency in the range direction; K_r and T_r are the chirp rate and the pulse duration; V_r is the average velocity and L_a is the antenna length. The length of the moving average (B_{mov}) is 200Hz. The size of one image block is $N_a \times N_r = 2048 \times 4644$. The Doppler parameter estimation must be completed using 2048 range lines for real-time processing. The image block is portioned into six chunks, each having size of $N_a \times N_{chunk} = 2048 \times 774$.

Fig. 4(a) shows the RADARSAT signals from the region around Vancouver provided in [1]. Fig. 4(b), Fig. 4(c) and Fig. 4(d) show the results of the respective chunks assessed by SNR, ρ_{dis} and ρ_{sym}. According to the distribution of the quality indexes versus the first estimated baseband Doppler centroid, the thresholds of ρ_{dis} and ρ_{sym} are set to 12.06%, and 6.79%, respectively. Actually, the unreliable estimation of baseband Doppler centroid usually occurs in the chunk with a large variation of their reflectivity. Only the estimation results $\hat{f}'_{\eta_c}(c)$ of the chunk c with qualified ρ_{dis} and ρ_{sym} are reserved, where c is the chunk index.

Given $C = 12$, let $\hat{\mathbf{y}} = [\hat{f}'_{\eta_c}(1) \quad \dots \quad \hat{f}'_{\eta_c}(C)]^T$ and

$$\mathbf{X} = \begin{bmatrix} 1 & 2 & \dots & C \\ 1 & 1 & \dots & 1 \end{bmatrix}^T. \quad (16)$$

Assume that the weighting matrix is given by

$$\mathbf{W} = \text{diag}([\gamma_1 \quad \gamma_2 \quad \cdots \quad \gamma_C]), \quad (17)$$

where γ_c is the SNR of chunk c. If the initial estimated baseband Doppler centroid is regarded as unreliable, γ_c is set to 0. For $\mathbf{b} = [m \ d]^T$, the WLS algorithm is then applied to derive the refined estimation, which is given by

$$\hat{\mathbf{b}} = (\mathbf{X}^T\mathbf{W}\mathbf{X})^{-1}\mathbf{X}^T\mathbf{W}\hat{\mathbf{y}}, \quad (18)$$

and the refined estimation results become $\tilde{\mathbf{y}} = \mathbf{X}\hat{\mathbf{b}}$. Fig. 5 shows the necessity of quality assessment and the effect of ρ_{sym}. In Fig. 5(a), all the initial estimates $\hat{f}'_{\eta_c}(c)$ from ACCC are given. In Fig. 5(b), the refined estimation results $\tilde{f}'_{\eta_c}(c)$ for $1 \le c \le C$ by the WLS algorithm are shown. The phenomenon of

incoherence in Fig. 5(a) is improved. Furthermore, the incoherent estimates of the chunks indicated by black rectangles are disqualified by ρ_{sym}. An accurate estimation of baseband Doppler centroid can be obtained after quality assessment and the WLS algorithm.

B. Selective Window and Weighted Combining

The estimation of Doppler centroid in (7) is easily distorted by noise and interference. Thus, if it is used directly, the detection of Doppler ambiguity will be wrong. To enhance the correctness of Doppler ambiguity detection, a technique named selective window is proposed. Define α_w as the ratio of the selective window size with respect to N_r. After range compression and generation of beat signal $s_{beat}(\tau,\eta)$, the sample $s_{beat}(\tau_0,\eta_0)$ with the strongest signal strength in one image block is chosen as a reference point and the selected sub-region of size $N_a \times \alpha_w N_r$ is defined, as shown by the yellow part in Fig. 6. Only the signals inside the selected sub-region are considered by the MLBF method to estimate $\hat{f}_{\eta_c}$ and then $\hat{M}_{amb}$ is detected.

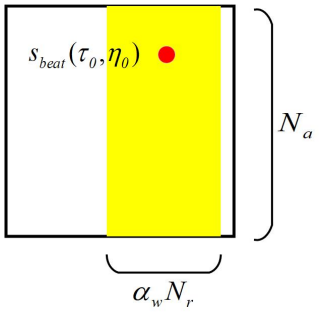

Fig. 6 Selective window in one image block.

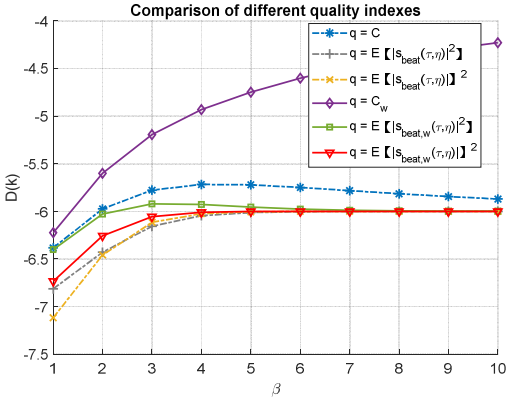

Fig. 7 Comparison of Doppler ambiguity estimation using different quality index.

In [1], the contast c is described as

$$c = E\{|s_{rc}(\tau,\eta)|^2\}/E\{|s_{rc}(\tau,\eta)|\}^2. \quad (19)$$

We first investigate weighted average by different quality indexes to derive the final detection result D of Doppler ambiguity,

$$D = \frac{\sum_{i=1}^{N} q(i)^{\beta} \hat{M}_{amb}(i)}{\sum_{i=1}^{N} q(i)^{\beta}}, \quad (20)$$

where $q(i)$ and $\hat{M}_{amb}(i)$ denote the quality index and the estimated Doppler ambiguity of the ith image block by MLBF. Fig. 7 shows the simulation results using different quality indexes versus the power β of the weighting factor for 16 image blocks ($N = 16$) in Fig. 4(a). The correct Doppler ambiguity is -6. The quality indexes include the contrast, the average power, and the square of the average amplitude of the beat signal $s_{beat}(\tau,\eta)$. The technique of the selective window is applied to the beat signal if subscript w is inserted. It is clear that we can obtain correct Doppler ambiguity by using $E\left\{\left|s_{beat,w}(\tau,\eta)\right|^2\right\}$ and $E\{|s_{beat,w}(\tau,\eta)|\}^2$ with small power β.

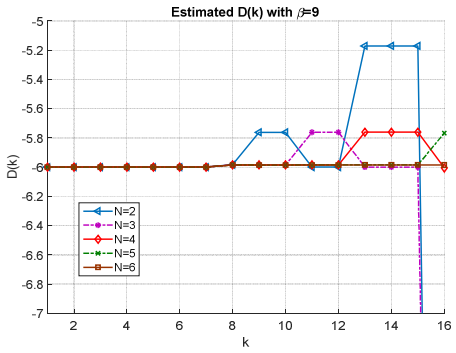

(a)

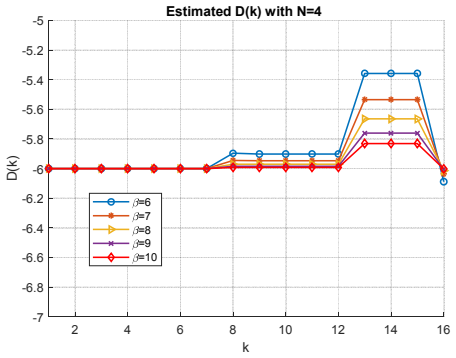

(b)

Fig. 8 Weighted combining and tracking of Doppler ambiguity with (a) different settings of N, and (b) different settings of β.

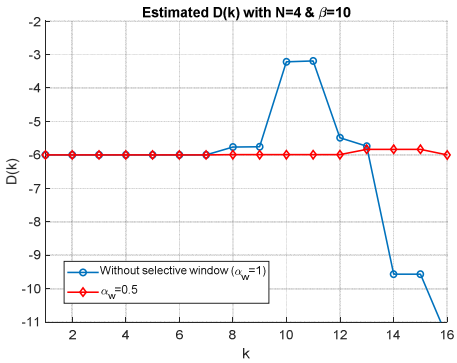

Fig. 9 Doppler ambiguity estimation with and without selective window.

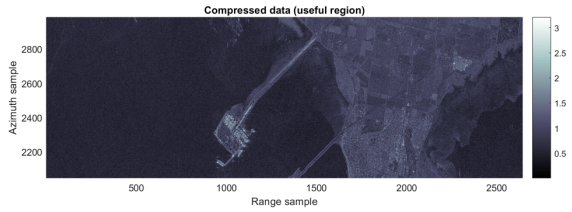

Fig. 10 SAR imaging with estimated Doppler centroid.

Taking advantage of slow-varying Doppler ambiguity, we then use selective combining to derive the final detection of Doppler ambiguity $D\left(k|\mathbf{q},\widehat{\mathbf{M}}_{\mathbf{amb}}\right)$ of the kth image block,

$$D\left(k|\mathbf{q},\widehat{\mathbf{M}}_{\mathbf{amb}}\right)=\begin{cases}\frac{\sum_{i=1}^{k}q(i)^{\beta}\widehat{M}_{amb}(i)}{\sum_{i=1}^{k}q(i)^{\beta}}, & k<N\\ \frac{\sum_{i=k-N+1}^{k}q(i)^{\beta}\widehat{M}_{amb}(i)}{\sum_{i=k-N+1}^{k}q(i)^{\beta}}, & k\geq N\end{cases}. \tag{21}$$

where $\mathbf{q}=[q(k)\ q(k-1)\ \dots\ q(k-N+1)]$ and $\widehat{\mathbf{M}}_{\mathbf{amb}}=[\widehat{M}_{amb}(k)\ \widehat{M}_{amb}(k-1)\ \dots\ \widehat{M}_{amb}(k-N+1)]$ are the quality indexes and estimated Doppler ambiguities of the previous image blocks. The quality index of $E\left\{\left|s_{beat,w}(\tau,\eta)\right|^2\right\}$ is employed in the following. Because the Doppler centroid is highly related with the squint angle, the sign of Doppler centroid will be the same as the sign of squint angle. Thus, if the estimated Doppler ambiguity $\widehat{M}_{amb}(i)$ is positive for this case with negative squint angle, it will be removed from the weighted combining. Furthermore, if the rough velocity and attitude measurement of the airborne can be obtained, the convergence can be accelerated by shrinking the possible estimation range of Doppler ambiguity.

Fig. 8 shows the combined results for different image blocks, $k=1,2,\dots,16$. Various N values are considered in Fig. 8(a) and it is sufficient to obtain correct Doppler ambiguity with $N\geq 4$. Fig. 8(b) depicts the effect of β given $N=4$. Fig. 9 provide the comparison of combined results with and without the selective window technique. Thus, the weighted combining and selective window technique can generate reliable Doppler ambiguity estimation with proper setting of N and β.

It has been mentioned in [1] that the error tolerance of Doppler centriod will be smaller than $\pm 7.5\%F_a$ to constrain the distortion. The error from Fig. 5(b) is about several to several tens Hz and can satisfy the critertion with $F_a=1257$. With our Doppler estimation results, the focused SAR image by the RDA algorithm is shown in Fig. 10. Hence, it demonstrates that the proposed scheme is feasible.

IV. Conclusion

In this paper, the estimation of Doppler centroid including baseband Doppler centroid and Doppler ambiguity is studied for real-time SAR imaging. The symmetry of Doppler spectrum is assessed in addition to the spectrum distortion, which can eliminate some unreliable estimations. The weighted least squares algorithm is then applied to the qualified estimates to derive the final result. The simulation results show the coherence of baseband Doppler centroid among the adjacent chunks. By exploiting the slow-varying properties of Doppler ambiguity, weighted combining and selective window techniques are used. In addition, the quality index of average power is more suitable than the contrast to weight the estimated Doppler ambiguity of each image block. The simulation results show the improvements compared to the conventional methods and the compressed SAR image based on the proposed processing flow of Doppler centroid estimation is given to demonstrate its feasibility.

References

[1] I. G. Cumming and F. H. Wong, Digital Processing of Synthetic Aperture Radar Data. Norwood, MA: Artech House, 2005.

[2] S. N. Mandsen, "Estimating the Doppler centroid of SAR data", *IEEE Trans. Aerosp. Electron. Syst.*, vol. 25, no. 2, pp. 134-140, Mar. 1989

[3] F. Wong, I. G. Cumming, "A combined SAR Doppler centroid estimation scheme based upon signal phase," IEEE Trans. Geosci. Remote Sens. 1996, 34, 696–707.

[4] L. Zhang, Y. Gao, X. Liu and L. Liu, "A novel method for estimating the baseband Doppler centroid of conventional synthetic aperture radar," 2017 IEEE International Geoscience and Remote Sensing Symposium (IGARSS), pp. 5426-5429.

[5] W. Li, J. Yang, Y. Huang, "Improved Doppler parameter estimation of squint SAR based on slope detection," Int. J. Remote Sens. 2014, 35, 1417–1431.

[6] J. Wang, J. Wu, W. Pu, W. Li, and J. Yang," A Doppler centroid estimator for synthetic aperture radar based on phase center point tracking.", 2018 IEEE International Geoscience and Remote Sensing Symposium (IGARSS), pp. 3679-3682.

[7] Zhonghua Chen et al. "On the Doppler centroid estimation of SAR system using coherence information" 2019 Asia-Pacific Conference on Synthetic Aperture Radar (APSAR), pp.1-4.